JOURNAL OF MATERIALS SCIENCE 27 (1992) 881–888

Oriented mosaic model analysis of anisotropic thermoelectric properties of heterogeneous materials

HIDEO WADA
Corporate Research and Development Centre of Mitsui Mining and Smelting Co. Ltd, 1333-2, Haraichi, Ageo-shi, Saitama 362, Japan

YOICHI OKAMOTO, TORU MIYAKAWA
Department of Materials Science and Engineering, The National Defense Academy, Yokosuka, Kanagawa 239, Japan

TAIZO IRIE
Department of Electrical Engineering, Science University of Tokyo, Kagurazaka, Shinjuku, Tokyo, 62, Japan

Thermoelectric properties of heterogeneous materials are discussed in terms of a randomly oriented rectangular plate-like mosaic of anisotropic crystalline grains embedded in a homogeneous host material. Anisotropies in effective thermoelectric parameters and the values of thermoelectric parameters can be related to the mean orientation of the plate-like grains which, in turn, can be related to the orientation factor of Lotgering. They are also functions of various parameters such as dimension ratios α, α' and α'' of electrical resistivities, thermal conductivities, and the Seebeck coefficient, respectively, of grains to those of host medium. Use of f-dependent anisotropies in conjunction with relative magnitudes of electrical and thermal conductivities as well as of the Seebeck coefficient, allows α, α' and α'' to be estimated, which characterize the intergranular medium.

1. Introduction

Heterogeneous materials, such as sintered or hot-pressed ceramics, are at the focus of increasing interest from both scientists and engineers. Aside from the great potentiality of high T_c superconducting ceramics [1], they are used in various fields of materials engineering.

In addition, the obvious merit from the cost-performance point of view is that they often exhibit improved mechanical properties over those of easily cleaved or brittle crystalline counterparts, as exemplified by the fibre-reinforced materials. Moreover, one may take advantage of the complex structure of these substances, i.e. the existence of grain boundaries or intergranular substances, to improve the effective performance of the system. One of the classical examples is the boundary layer capacitance (e.g. [2]). Also ZnO varistors [3] PTC semiconducting ceramics [4] are believed to make use of properties of boundary layer junctions, though this is not yet well understood.

Material design of heterogeneous systems with their optimal characteristics is a challenging task. However, endeavour in this direction has largely been empirical in nature and almost no systematic attempt seems to have been made so far to understand or control the characteristics of a specific heterogeneous system. This is because there are so many processing parameters which influence the "microscopic" structure of the system which, in itself, is very complex and cannot be simply characterized. The second difficulty seems to be related to the fact that there are so many physical parameters characterizing each "microscopic" member of the system, many of which cannot be measured separately. Finally, there has been no simple recipe established to relate these parameters to the effective bulk physical parameters of the system.

The effective medium theory (EMT) seems to be one of the most promising ways to predict the effective parameters of the overall system from those of the constituent members. It gives effective physical parameters, such as conductivity [5, 6], susceptibility [7, 8], elastic constants [9], or optical constants [10] of the system in terms of those of component materials and also of their ratios in spatial dimensions. In this kind of theory the heterogeneous system is modelled either as a homogeneous medium into which spherical [11], cylindrical [12], or ellipsoidal [13] particles of the second medium are embedded. From the self-consistency requirement, usually expressed in the form of boundary conditions at the surface of these embedded particles, effective physical parameters can be determined.

Sophisticated expressions are derived [14], or lower or upper bounds are given for the effective parameters in the iterative solution of these implicit expressions for the parameters [15]. In some cases, the statistical

distributions of particles are taken into account [16, 17].

Unfortunately, these theories are much too sophisticated to compare their results with a large compilation of experimental data. The theories are also built only to simulate the "effective conductivity tensors" and, to our knowledge, only one preliminary report has been made on an attempt to discuss thermoelectric power of the system [18].

On the other hand, a simple square mosaic model originally proposed by Volger [19] to discuss Hall voltage has been extended to the discussion of not only conductivity but also Hall and Seebeck coefficients of heterogeneous systems by Bube [20, 21] in an attempt to discriminate between barrier and number mechanisms of photoconductivity in PbS films [22].

In this paper, we extend this approach to the case of a randomly oriented plate-like mosaic model to simulate the anisotropic thermoelectric properties of hot-pressed Bi_2Te_3 semiconducting ceramics. Bi_2Te_3 thermoelectric ceramics are chosen because they can be characterized by the famous figure of merit Z [23]. Also, hot-pressed samples in this system have recently been shown to exhibit a competitive figure of merit, Z, compared to that of zone-melted samples and it is of interest to try to give a guide to optimize Z of this system [24].

In the following sections, models, assumptions and approximations are given. Expressions for the effective conductivities and Seebeck coefficient of the heterogeneous sample are given which are then used in the numerical studies outlined. The results are discussed and qualitative comparison is made with the experimental data on the Bi_2Te_3 system [25].

2. Experiments and results

2.1. Sample preparation

The bromine-doped $Bi_2Te_{2.85}Se_{0.15}$ alloys were melted in a 1 atm Ar atmosphere at 800 °C for 3–5 h. The zone-melted samples were grown in a quartz tube of 25 mm diameter moving in one direction at a rate of 5 mm h^{-1}. The alloys for the hot-pressed samples were cooled slowly and crushed in a stamp mill in a non-volatile atmosphere. They were then sifted into five groups of grains with diameters ranging from about 50–250 μm. The powders thus prepared for sintering were hot-pressed at 500 °C under 300 kgf cm^{-2} ($\sim 2.9 \times 10^3$ N cm^{-2}) for 1 h. The zone-melt and hot-pressed samples were prepared in the form of a platelet with dimensions $5 \times 15 \times 3$ mm^3. Measurements were made on these samples.

2.2. Thermoelectric measurements and X-ray diffraction

Fig. 1 shows the direction of the measurements for Seebeck coefficient, S, and the electrical resistivity, $\rho(\sigma^{-1})$, of the hot-pressed and zone-melted samples. Seebeck coefficient, S, was measured at 300 K by the standard d.c. technique using a thermal belt sensor made of a thin film of copper–constantan [23]. This sensor enabled us to measure the Seebeck coefficient

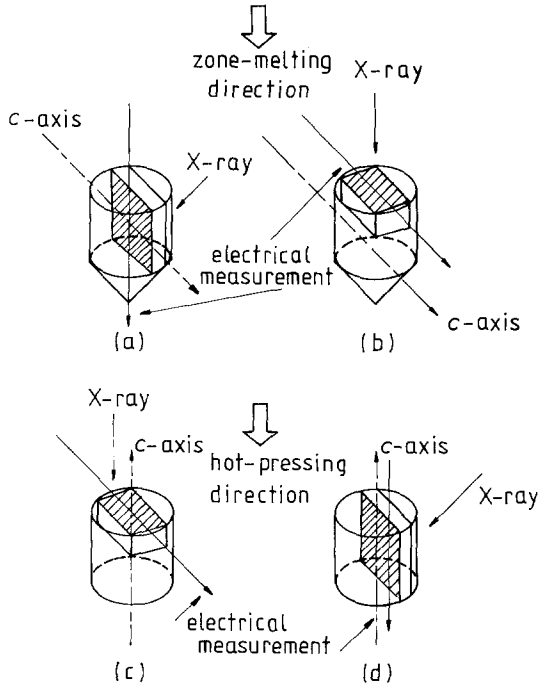

Figure 1 Sample and measurement configuration. (a) Zone-melted c-plane direction sample: direction of measurement is in the plane of the sample and is perpendicular to the hot-pressed direction. (b) Zone-melted c-axis sample: direction of measurement is in the plane of the sample and parallel to the hot-pressed direction. (c) Hot-pressed c-plane direction sample: direction of measurement is in the plane of the sample and is parallel to the zone-melting direction. (d) Hot-pressed c-axis sample: direction of measurements is in the plane of the sample and perpendicular to the zone-melting direction.

of the sample with ± 5 μV K^{-1} accuracy. Electrical resistivity, ρ, was measured using two probes separated by 2 mm, reversing the direction of the current with a turning switch. The temperature dependence of conductivity was measured using an a.c. technique using an LCR meter in a sealed evacuated chamber cooled with liquid nitrogen.

Fig. 2 shows the X-ray diffraction patterns of the zone-melted and hot-pressed samples. In the case of the zone-melted sample, the X-ray diffraction intensities of the $(0, 0, l)$ directions are strong perpendicular to the zone-melting direction, while in the case of hot-pressed samples, they are strong in the hot-pressed direction. The a-axis of the zone-melted sample is oriented along zone-melting direction.

Generally, hot-pressed $Bi_2Te_{2.85}Se_{0.15}$ samples consist of flake-like grains whose normal c-axes are oriented randomly around the pressed direction. The average orientation of microcrystallites in the samples is estimated from the X-ray diffraction intensities of the $(0, 0, l)$ planes.

According to Lotgerling [26], the orientation factor, f, is defined by

$$f = (P - P_0)/(1 - P_0) \quad (1)$$

where P is the fraction of diffraction intensity, $I(0, 0, l)$ from the $(0, 0, l)$ planes to the total intensities, $\Sigma I(h, k, l)$, given as

$$P = \Sigma I(0, 0, l)/\Sigma I(h, k, l) \quad (2)$$

where P_0 is the value of P for the sample which shows

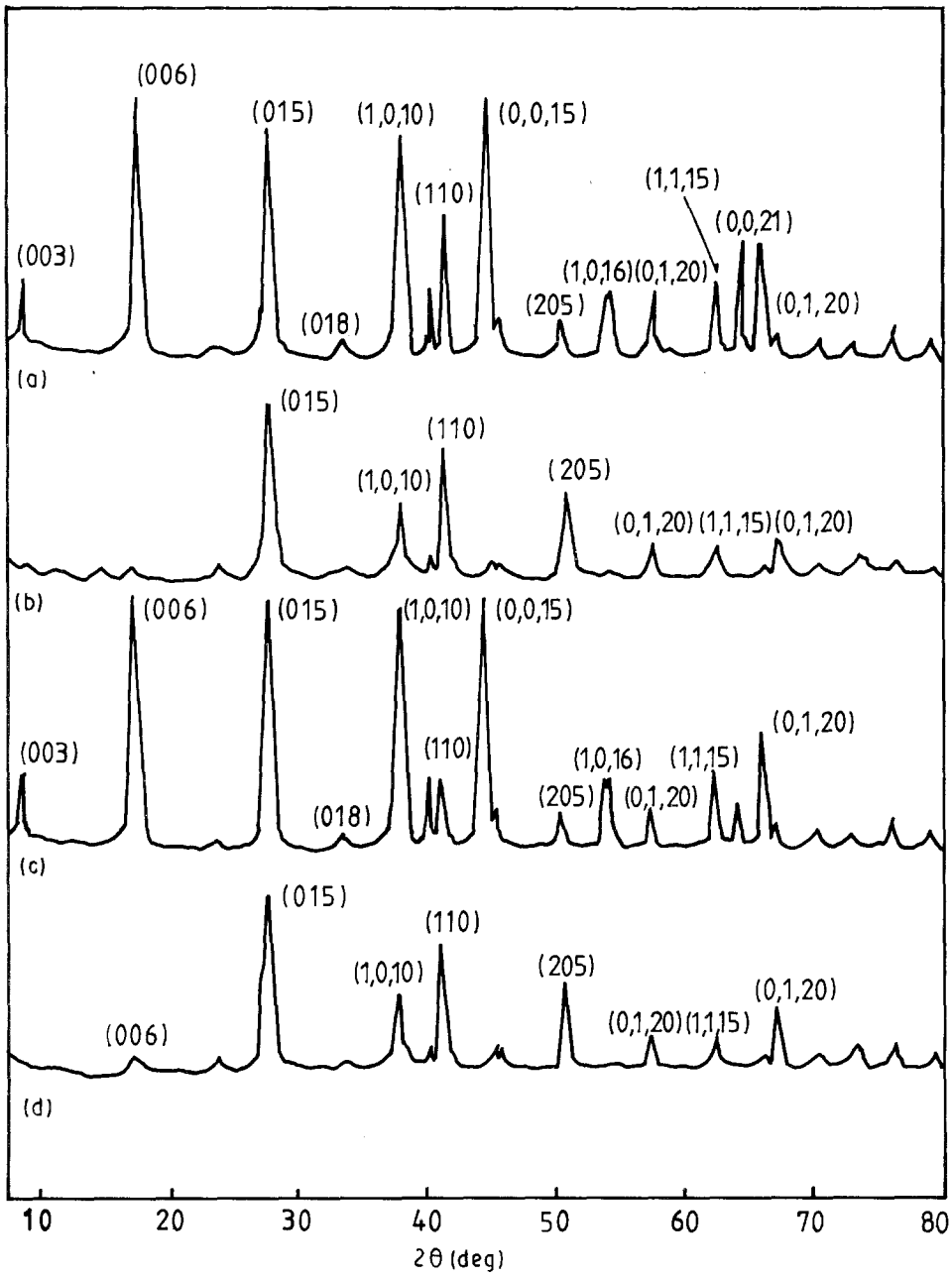

Figure 2 X-ray diffraction pattern for $Bi_2Te_{2.85}Se_{0.15}$ for (a) hot-pressed c-plane direction sample, (b) hot-pressed c-axis direction sample, (c) zone-melted c-plane direction sample, (d) zone-melted c-axis direction sample.

no preferential orientation. We have used the P value of the unpressed sample as our standard P_0 [11].

Table I shows the thermoelectric properties of Seebeck coefficients, S, electrical conductivities, σ, the densities, and the orientation factor, f, of the zone-melted and the hot-pressed samples. The Seebeck coefficients and electrical conductivities of the zone-melted samples were higher than those of hot-pressed samples. The orientation factor shows the same tendency. In this case, the thermoelectric properties of the hot-pressed samples were found to be close to those of the zone-melted samples without degradation of its Seebeck coefficient. Table II shows the anisotropy of σ, κ and S, respectively. It is well known that crystalline grains in the zone-melted samples show cleavage along planes perpendicular to the c-axis. The

TABLE I The thermoelectric properties of zone-melted sample and hot-pressed sample

Sample	Zone-melting and hot-pressing conditions	Density ($g\,cm^{-3}$)	Orientation factor, f	Conductivity, $\sigma(\Omega^{-1}\,cm^{-1})$	Seebeck coefficient, $S(\mu V\,K^{-1})$	$\alpha^2\sigma$ ($10^{-3}\,W\,cm\,K^{-2}$)
Zone-melted sample	800 °C, 5 mm h^{-1} (zone-rate)	7.70	0.932	1.00	205	42.0
Hot-pressed sample	$T = 500$ °C, 60 min $P = 300\,kgf\,cm^{-2}$	7.62	0.756	0.97	198	38.0

TABLE II The thermoelectric properties of zone-melted samples and hot-pressed samples for $Bi_2Te_{2.85}Se_{0.15}$

Sample	Direction	Seebeck coefficient, $S(\mu V K^{-1})$	Thermal conductivity, κ (mW cm^{-1} K^{-1})	Electrical conductivity, $\sigma(\rho^{-1})$ (Ω^{-1} cm^{-1})	Thermoelectrical figure of merit (10^{-3} K^{-1})
Zone-melted	c-plane	215	17.6	1.08	2.85
sample	c-axis	236	15.2	0.31	1.14
Anisotropic		$\gamma''(S_{\parallel}/S_{\perp})$	$\gamma'(\kappa_{\parallel}/\kappa_{\perp})$	$\gamma(\rho_{\parallel}/\rho_{\perp})$	$g(Z_{\parallel}/Z_{\perp})$
factor		0.91	1.16	0.29	2.50
Hot-pressed	c-plane	200	14.9	1.05	2.83
sample	c-axis	198	11.0	0.56	1.98
Anisotropic		$\Gamma''(S_F/S_Z)$	$\Gamma'(\kappa_F/\kappa_Z)$	$\Gamma(\rho_F/\rho_Z)$	$G(Z_F/Z_Z)$
factor		1.03	1.35	0.53	1.43

Hot-pressing conditions: $T_p = 60$ min, $P = 300$ kg cm^{-2}, $T_h = 500$ °C, particle sizes 250–150: 150–90: 90–75 = 1:2:1.
Zone-melting conditions: 800 °C, 5 mm h^{-1} (zone-rate).

TABLE III Analysis of imaging of the optical micrograph for $Bi_2Te_{2.85}Se_{0.15}$

Sample		Area (μm^2)	Circle diameter (μm)	Ellipse diameter (μm)		Ellipticity (a/c)
				a (long diameter)	c (short diameter)	
c-plane	Min.	1.00	1.13	0.0	0.0	–
	Max.	5.18×10^3	8.12×10^1	1.05×10^2	7.01×10^1	1.49
	Ave.	5.11×10^3	2.21×10^1	3.23×10^1	1.56×10^1	2.07
c-axis	Min.	2.37	1.74	0.0	0.0	–
	Max.	2.19×10^4	1.67×10^2	3.57×10^2	1.48×10^2	2.40
	Ave.	1.58×10^3	3.60×10^1	6.77×10^1	2.06×10^1	3.29

parameter with the strongest anisotropy is σ and its magnitude $\sigma_{\parallel}/\sigma_{\perp}$ amounts to 2.5 for the zone-melted sample.

2.3. The imaging analysis and aspect ratio of the grains

Fig. 3 shows the block diagram of the system for micrograph image analysis of the cross-section of hot-pressed samples. Observations by optical microscopy were made after polishing the surface of the sample with carborundum powder (no. 2000) and then chemically etching the surface in ethyl alcohol with HNO_3 for 3 min. The optical micrographs were displayed on a TV monitor. The displayed image pictures were fixed and their ratio of areas was measured by the contrast between boundaries and grains from the image of their optical micrograph in TVIP-2000. From the measurements, the distribution of particle sizes and the approximate value of anisotropy were calculated using a personal computer. Their estimated minimum, maximum and average values are indicated in Table III.

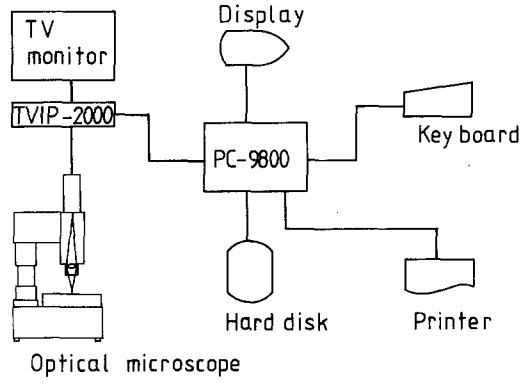

Figure 3 The block diagram of the image analysis of a micrograph of hot-pressed samples.

Fig. 4 shows the imaging analysis of the micrographs of the c-plane and c-axis in the hot-pressed sample. In the c-plane sample, platelet patterns of the particles were observed and several particles exist in the c-axis sample. Table III gives the results of the imaging analysis of the grains and the grain boundary. The ratio of grains to the grain-boundary area was estimated to be about 95%, which is similar to the densities of the sintered samples. Fig. 5 shows the distribution of the areas of grains. From Table III it can be seen that the ratio of average ellipticity (a/c) for the c-axis sample is 1.6 times that of c-plane sample. If one assumes that one is looking at a random distribution of pancake-like (oblate) ellipsoids of revolution with their average larger and smaller semiaxes a and c from the F and Z directions one can estimate both the mean ellipticity

$$\varepsilon \equiv c/a \tag{3}$$

and average of $\cos^2\theta$

$$X = \langle \cos^2\theta \rangle \tag{4}$$

from these observations (Fig. 6). Employing the approximation $\langle (X^2 + Z^2)/c_z^2 \rangle \sim \langle X^2 + Z^2 \rangle / \langle c_z^2 \rangle$ we arrive at ($c'_1 = c_{\parallel}$ or $c_{\perp}$)

$$(c_{\perp}/a)^2 = \frac{\varepsilon^2}{\varepsilon^2 + (1 - \varepsilon^2) X} \tag{5}$$

$$(c_{\parallel}/a)^2 = \frac{\varepsilon^2}{1 + (\varepsilon^2 - 1) X} \tag{6}$$

We estimate $\varepsilon = 0.28$ and $X = 0.78$ for this sample from the experimental data.

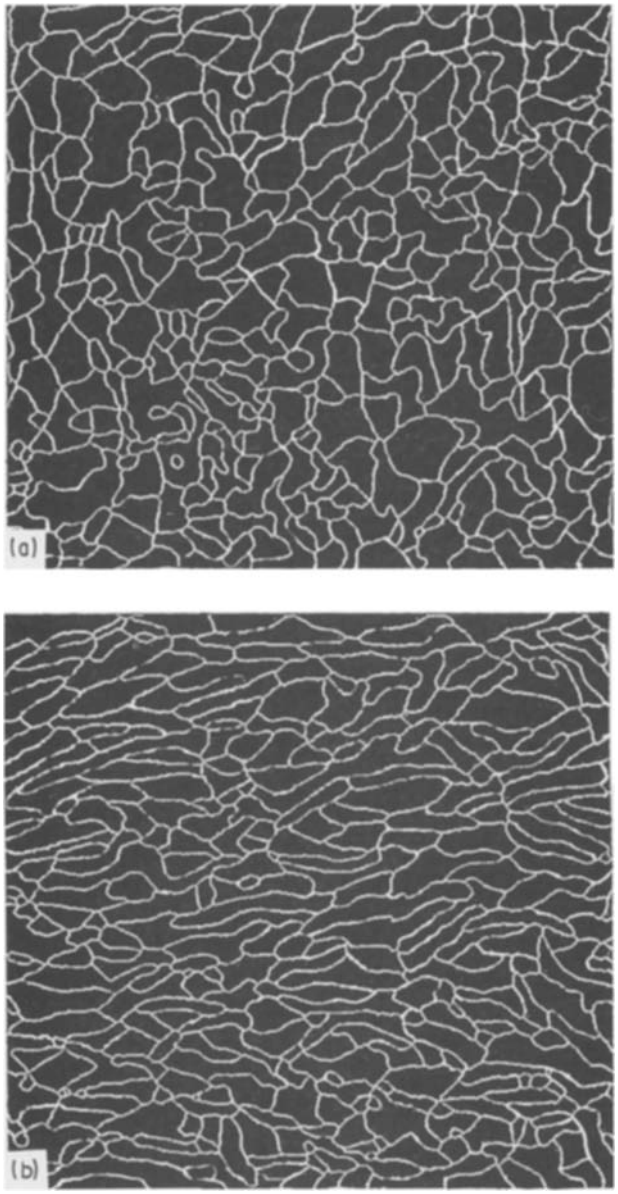

Figure 4 Imaging analysis of the micrographs of the hot-pressed samples. (a) Cross-section perpendicular to pressed direction, (b) cross-section parallel to pressed direction. $T_h = 500\,^{\circ}C$, $P_h = 300\,kg\,cm^{-2}$.

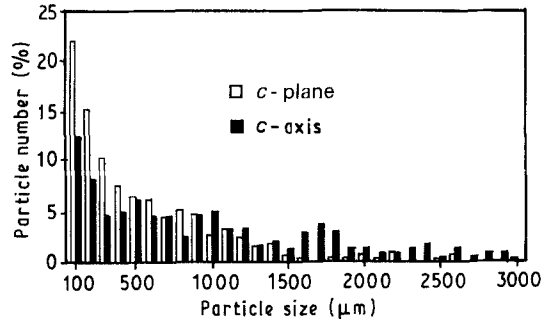

Figure 5 The distribution of cross-sectional areas of the grains in a hot-pressed sample.

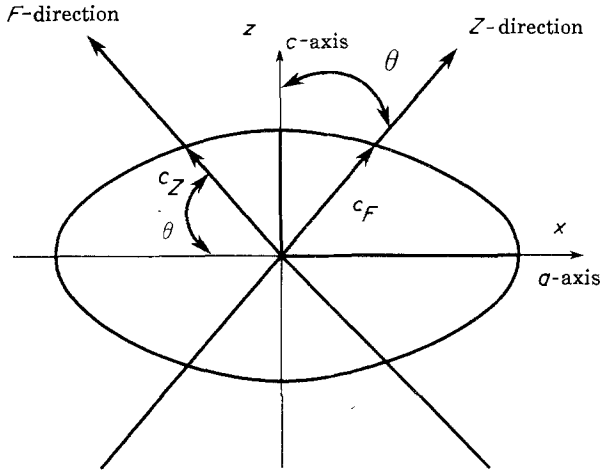

Figure 6 Imaging analysis of the grain size for the orientation factor, *f*. *a* is the major axis and c_Z, c_F are the minor axes in the parallel and perpendicular directions.

3. Theory

3.1. Three-dimensional mosaic model and approximations

Contrary to the case of ZnO varistors, no evidence is known to suggest the importance of characteristics related to the non-linear or junction nature of the interface between grains and intergranular medium in our system. Therefore, the simplest mosaic model was adopted in which no such non-linear effects are incorporated. Fig. 7 shows our three-dimensional mosaic model. In this model, thin, square ($l_0 \times l_1 \times l_1'$) plate-like grains with anisotropic parameters are embedded in an isotropic homogeneous intergranular medium 2 of thickness l_2, resistivity ρ_2, thermal conductivity κ_2, and Seebeck coefficient S_2. Crystalline grains are, in general, anisotropic and are characterized by ρ_1, $\gamma\rho_1$; κ_1, $\gamma'\kappa_1$; S_1, $\gamma''S_1$ in the direction along and perpendicular to the *c*-axis. Stacks of the blocks consisting of the grain and the surrounding intergranular medium are arranged in a random fashion with their azimuthal θ and meridian ϕ angles distributed according to some statistical distribution. We assume that the distribution in ϕ is uniform so that $\langle\cos^2\phi\rangle = \langle\sin^2\phi\rangle = 1/2$, while the distribution in θ is affected by the hot-pressing process. We can expect that $\langle\cos^2\theta\rangle$ is related to the orientation factor of Lotgering. In the absence of precise information on the statistical distribution of θ, we assume a simple linear relation

$$X = \langle\cos^2\theta\rangle = (1 + 2f)/3 \tag{7}$$

We have also made the approximation

$$X' = \langle\cos^4\theta\rangle = (1 + 2f + 2f^2)/5 \tag{8}$$

These approximate expressions are the outcome of the linear approximation and the "boundary condition" $X = X' = 1$ for $f = 1$ (perfect orientation) and $X = 1/3, X' = 1/5$ for $f = 0$ (uniform random orientation). Also we assume a quadratic relation $X' = aX^2 + b'$.

Anisotropy factors of crystalline grains $\gamma = \rho_{1\perp}/\rho_{1\parallel}$, $\gamma' = \kappa_{1\perp}/\kappa_{1\parallel}$, $\gamma'' = S_{1\perp}/S_{1\parallel}$ for resistivity, thermal conductivity, and Seebeck coefficient, respectively, may be estimated from the data on melt-grown samples. Geometrical factors $\beta = l_2/l_1$, $\beta' = l_0/l_1$ can also be estimated from the data on the imaging analysis of

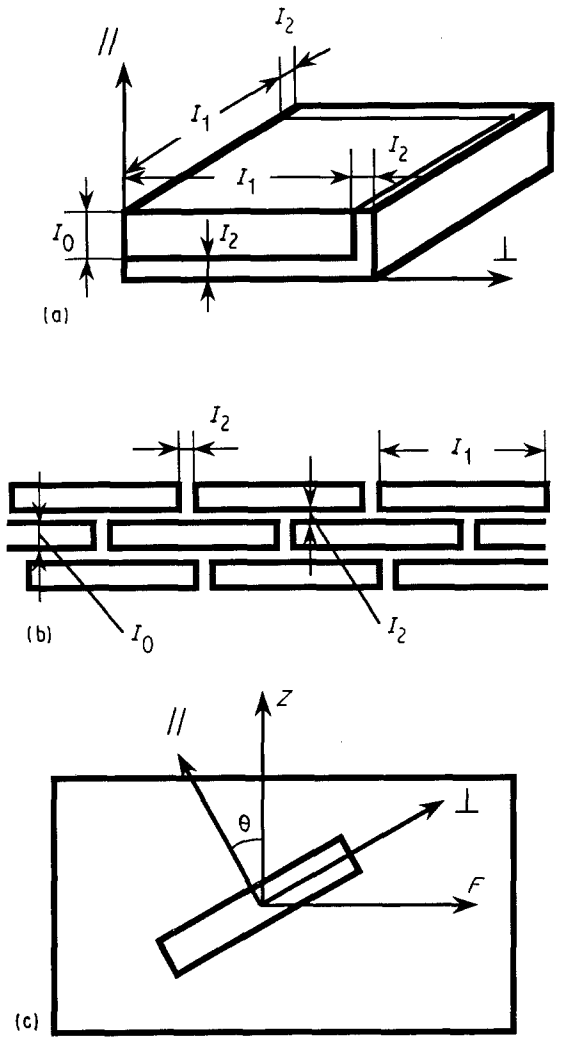

Figure 7 Three-dimensional mosaic model. (a) A block consists of a grain and intergranular medium, (b) stack and (c) random orientation of stacks. In this model, thin, square ($l_0 \times l_1 \times l_1'$) plate-like grains with anisotropic parameters are embedded in an isotropic homogeneous intergranular medium 2 of thickness l_2, resistivity ρ_2, thermal conductivity κ_2 and Seebeck coefficient S_2. Geometrical factors $\beta = l_2/l_1$, $\beta' = l_0/l_1$, can also be estimated from the data on imaging analysis of the micrographs.

the micrographs of the cross-sections of hot-pressed samples. β' may be identified with ε, as estimated in Section 2.3. Thus, $\alpha = \rho_1/\rho_2$, $\alpha' = \kappa_1/\kappa_2$, and $\alpha'' = S_1/S_2$ are the only parameters which may be adjusted to fit the data for the effective thermoelectric parameters of the ceramics.

In this simple model the important role played by voids or porosity of the sample is not included explicitly. Such effects or possible effects of grain interface structure can only be included through α.

3.2. Effective thermoelectric parameters

One can easily derive analytical expressions for the effective bulk thermoelectric parameters in parallel (P) and perpendicular (S) directions to the c-axis of the stacked layer of grains. Normalized expressions for thermoelectric parameters, resistivities, thermal conductivities and Seebeck coefficients can be written in terms of α and β:

Effective resistivity

$$\rho_P/\rho_1 = (1+\beta)^2(\beta+\alpha\beta')[\alpha(\beta+\beta') + \alpha\beta(2+\beta)(\alpha\beta'+\beta)] \quad (9)$$

$$\rho_S/\rho_1 = (1+\beta)(\beta+\beta')(\gamma\alpha+\beta)/[\alpha\beta'(1+\beta) + \alpha\beta(\gamma\alpha+\beta)(1+\beta+\beta')] \quad (10)$$

Effective thermal conductivity

$$\kappa_1/\kappa_P = \alpha'(1+\beta)^2(\beta'+\alpha'\beta)/[\alpha'(\beta+\beta') + \beta(2+\beta)(\beta'+\alpha'\beta)] \quad (11)$$

$$\kappa_1/\kappa_S = \alpha'(1+\beta)(\beta+\beta')(1+\gamma'\alpha'\beta)/[\gamma'\alpha'\beta'(1+\beta)+\beta(1+\gamma'\alpha'\beta) \times (1+\beta+\beta')] \quad (12)$$

Effective Seebeck coefficient

$$S_P/S_1 = [\beta' + \alpha''^{-1}\beta\{\alpha\beta'(2+\beta) + \langle\alpha\beta(2+\beta) + 1\rangle\alpha'\}]/(\beta'+\alpha'\beta)\{1+\alpha\beta(2+\beta)\} \quad (13)$$

$$S_P/S_1 = [\gamma''\beta' + \alpha''^{-1}\beta\{\gamma\alpha(1+\gamma'\alpha'\beta) \times (1+\beta+\beta') + \gamma'\alpha'\beta'\}]/(1+\gamma'\alpha'\beta) \times \{\beta' + \gamma\alpha\beta(1+\beta+\beta')\} \quad (14)$$

Next, we imagine that these stacks of grains and intergranular particles are oriented at random with a statistical distribution of θ and ϕ determined by the hot-pressing condition. The expression for statistically averaged thermoelectrical parameters in the Z and F directions parallel and perpendicular, respectively, to the pressed direction, can be found.

Average conductivity

$$\sigma_Z = \sigma_S + 2\Delta\sigma X \quad (15)$$

$$\sigma_F = \sigma_a - \Delta\sigma X \quad (16)$$

$$\sigma_a = (\sigma_P + \sigma_S)/2, \quad \Delta\sigma = (\sigma_P - \sigma_S)/2 \quad (17)$$

Average thermal conductivity

$$\kappa_Z = \kappa_S + 2\Delta\kappa X \quad (18)$$

$$\kappa_F = \kappa_a - \Delta\kappa X \quad (19)$$

$$\kappa_a = (\kappa_P + \kappa_S)/2, \quad \Delta\kappa = (\kappa_P - \kappa_S)/2 \quad (20)$$

Average Seebeck coefficient

$$S_Z = S_S + (\bar{S} - 2S_S)X + (S_P + S_S - \bar{S})X' \quad (21)$$

$$S_F = [3(S_P + S_S) + \bar{S} + 2(S_S - 3S_P + \bar{S})X + 3(S_P + S_S - \bar{S})X']/8 \quad (22)$$

$$\bar{S} = (S_P/\kappa_P)\kappa_S + (S_S/\kappa_S)\kappa_P \quad (23)$$

In the analysis of average Seebeck coefficients, we have used the fact that during the measurement of these coefficients, heat flows only along the direction of measurement. Also, we have extended our previous analysis [24] of the average Seebeck coefficients S_Z and S_F and employed an improved version of the approximation on $\langle\cos^4\theta\rangle$.

Even when the grains are isotropic, the effective thermoelectric parameters exhibit anisotropy in this model. The anisotropy will be stronger for smaller aspect ratio $\beta' = l_0/l_1$ for larger deviations from unity of anisotropy ratios, γ, of the grains. It grows as f increases. From the analytical expressions for the isotropic case we can show that the thermoelectric parameters of the mosaic sample should be intermediate between those of the grains and of the intergranular medium. This statement is also valid for the thermoelectric parameters of the stacks in the P or S direction.

3.3. Numerical analysis of the thermoelectric effect

From the experimental thermoelectric data on the zone-melted sample in Table II, the results of image analysis, and the anisotropy geometrical factors in Table III, we can estimate $\gamma = 0.3$, $\gamma' = 1.2$, $\gamma'' = 0.9$, $\beta = 0.03$, $\beta' = 0.28$ $(=\varepsilon)$. Fig. 8 shows an example of numerical analysis of the dependence of normalized thermoelectric parameters on the orientation factor, f, using these values and $\alpha = 2$, $\alpha' = 2$, $\alpha'' = 1.5$ in Equations 15–23. Rather strong f-dependence of conductivities σ_F, σ_Z and less sensitive behaviour of other parameters reproduce the experimental data on hot-pressed ceramics prepared under various processing conditions. Also, the fact that both σ_F and κ_F increase with f while S_F decreases slowly is in agreement with the experimental data. If one replaces the linear relation $X = (1 + 2f)/3$ with the quadratic one $(=(1 + 2f^2)/3)$, the straight lines in this figure will be replaced by parabolas with the same end points. Moreover, the anisotropy in ρ, κ, S and thermoelectric figure of merit, Z, can be simulated almost quantitatively by the deliberate choice of the parameter ratios α, α' and α''. With $\alpha = 2$, $\alpha' = 2$, $\alpha'' = 1.5$ (Fig. 8) the anisotropy in the averaged thermoelectric parameters may be obtained.

$$\Gamma \equiv \sigma_Z/\sigma_F = (\rho_F/\rho_Z) = 0.54 \quad (24)$$

$$\Gamma' \equiv \kappa_F/\kappa_Z = 1.1 \quad (25)$$

$$\Gamma'' \equiv S_F/S_Z = 1.03 \quad (26)$$

$$G \equiv Z_F/Z_Z = 1.43 \quad (27)$$

These values were derived from Fig. 8 for orientation factor $f = 0.67$ (dashed vertical line) estimated from the image analysis results using the approximate linear relation $X = (1 + 2f)/3$.

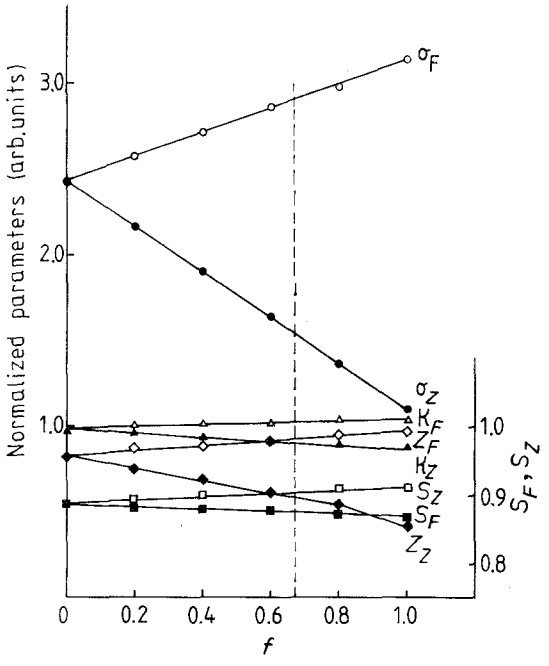

Figure 8 The results of numerical analysis on the dependence of normalized thermoelectric parameters σ_F/σ_1, σ_Z/σ_1, κ_F/κ_1, κ_Z/κ_1, S_F/S_1, S_Z/S_1 on the orientation factor, f.

4. Discussion

Reasonable agreement of these values with those listed in Table II offers the possibility of estimating parameter ratios α, α' and α'' from the analysis of anisotropies in the averaged thermoelectric parameters for the thermal conductivity, κ, and Seebeck coefficient, S. The crystalline anisotropies γ' and γ'' are not far from unity and geometrical anisotropy, which is sensitive to the value of α' or α'', gives sizeable contribution to the anisotropy of the averaged parameter. On the contrary, small values of γ make the contribution of physical anisotropy dominant, so that the ratio $\Gamma \equiv \sigma_Z/\sigma_F$ is primarily determined by f and is rather insensitive to α. In this case, one must also use the magnitude of σ_F or σ_Z in the estimate of α. These values of α, α' and α'' may be used in optimizing the thermoelectric figure of merit, Z, by means of an equal-Z-contour map on the α'' versus $\alpha^{1/2}\alpha'$ plane [24].

Unfortunately, the decrease in conductivities for samples with lower values of f is far more rapid than this model predicts. This seems to be related to a lower density in these samples, apparently associated with the presence of voids. In such cases, one may use effective α values which decrease rapidly as f becomes small.

5. Conclusion

The anisotropic thermoelectric properties of hot-pressed and zone-melted samples of n-type $Bi_2Te_{2.85}Se_{0.15}$ were measured and analysed in terms of an oriented mosaic model. Ratios of grains and boundary-layer dimensions and anisotropy ratios of thermoelectric parameters of crystalline grains were estimated from the microscopic image analysis of the sample cross-section and from measurement of thermoelectric parameters of grains in two orthogonal directions. Using these ratios, an oriented mosaic model is shown to be capable of predicting the anisotropy of averaged thermoelectric parameters of a hot-pressed sample with a specified orientation factor, f, with reasonable accuracy. The estimate of these parameters gives valuable information in optimizing the figure of merit of hot-pressed effects of c-axis and c-plane samples. The thermoelectric properties of the hot-pressed $Bi_2Te_{2.85}Se_{0.15}$, when a deliberate choice is made of parameters α, α' and α'', characterize the physical characteristics of the boundary layer.

Acknowledgements

The authors thank Associate Professor Jun Morimoto, National Defense Academy, for valuable discussions.

References

1. J. G. BEDNORTZ and K. A. MÜLLER, *Z. Phys.* **B64** (1986) 189.
2. R. L. WILLIAMSON, R. N. WRIGHT, G. E. KORTH and B. H. RABIN, *J. Appl. Phys.* **66** (1989) 1826.
3. S. WAKU, *J. Electro. Commun. Soc. Jpn* **49** (1966) 1285, in Japanese.
4. L. M. LEVINSON and H. R. PHILLIPP, *J. Appl. Phys.* **46** (1975) 1332.
5. W. HEYWANG, *J. Amer. Cer. Soc.* **47** (1964) 484.
6. A. K. SEN and S. TORQUATO, *Phys. Rev.* **B39** (1989) 4505.
7. S. TORQUATO and A. K. SEN, *J. Appl. Phys.* **67** (1990) 1145.
8. Z. HASHIN and S. STRIKMAN, *ibid.* **33** (1962) 3125.
9. P. CHYLEK and V. SRIVASTAVA, *Phys. Rev.* **B27** (1983) 5098.
10. J. G. BERRYMAN, *J. Appl. Phys.* **59** (1986) 1136.
11. G. BOSI, F. E. GIROUARD and V. TRUONG, *ibid.* **53** (1982) 648.
12. A. S. SANGANI and A. ACRIVOS, *Proc. R. Soc. Lond.* **A386** (1983) 263.
13. Y. BENVENISTE, T. CHEU and G. J. DVORAK, *J. Appl. Phys.* **67** (1990) 2878.
14. J. W.HAUS, R. INGUVA and C. M. BOWDEN, *Phys. Rev.* **A40** (1989) 5729.
15. Y. BENVENISTE and T. MILOH, *J. Appl. Phys.* **66** (1989) 176.
16. J. F. THOVERT, I. C. KIM, S. TORQUATO and A. ACRIVOS, *ibid.* **67** (1990) 6088.
17. A. S. SANGANI and C. YAO, *ibid.* **63** (1988) 1334.
18. A. B. KAISE, *Phys. Rev.* **B40** (1989) 2806.
19. J. VOLGER, *ibid.* **79** (1950) 1023.
20. R. H BUBE, *Appl. Phys. Lett.* **13** (1968) 136.
21. *Idem., ibid.* **14** (1969) 84.
22. G. D. MAHAN, *J. Appl. Phys.* **65** (1989) 1578.
23. H. WADA, T. SATO, K. TAKAHASHI and N. NAKATSUKASA, *J. Mater. Res.* **5** (1990) 1052.
24. H. WADA, Y. OKAMOTO, T. MIYAKAWA and T. IRIE, in "Proceedings of the International Conference on Computer Application in Materials Science and Engineering" (CAMSE' 90) Tokyo (1990).
25. T. MIYAKAWA, H. WADA and T. IRIE, *Mem. N.D.A* **28** (1990) 287.
26. F. K. LOTGERING, *J. Inorg. Nucl. Chem.* **9** (1959) 113.

Received 18 October 1990
and accepted 25 February 1991